NJC

Accepted Manuscript

This is an *Accepted Manuscript*, which has been through the Royal Society of Chemistry peer review process and has been accepted for publication.

Accepted Manuscripts are published online shortly after acceptance, before technical editing, formatting and proof reading. Using this free service, authors can make their results available to the community, in citable form, before we publish the edited article. We will replace this *Accepted Manuscript* with the edited and formatted *Advance Article* as soon as it is available.

You can find more information about *Accepted Manuscripts* in the Information for Authors.

Please note that technical editing may introduce minor changes to the text and/or graphics, which may alter content. The journal's standard Terms & Conditions and the Ethical guidelines still apply. In no event shall the Royal Society of Chemistry be held responsible for any errors or omissions in this *Accepted Manuscript* or any consequences arising from the use of any information it contains.

ROYAL SOCIETY OF CHEMISTRY

www.rsc.org/njc

Cite this: DOI: 10.1039/c0xx00000x

www.rsc.org/xxxxxx

ARTICLE TYPE

Energy efficient microwave synthesis of mesoporous $Ce_{0.5}M_{0.5}O_2$ (Ti, Zr, Hf) nanoparticles for low temperature CO Oxidation in an ionic liquid- a comperative study

Tarek Alammar,[a] Ying-Kit Chow,[a,b] Anja-Verena Mudring*[a,c]

Received (in XXX, XXX) Xth XXXXXXXXX 20XX, Accepted Xth XXXXXXXXX 20XX
DOI: 10.1039/b000000x

$Ce_{0.5}M_{0.5}O_2$ (M=Ti,Zr, Hf) nanoparticles have been successfully synthesized by microwave irradiation in the ionic liquid $[C_4mim][Tf_2N]$ (1-butyl-3-methylimidazolium bis(trifluoromethanesulfonyl)amide). The morphology, crystallinity, and chemical composition of the obtained materials were characterized by scanning electron microscopy (SEM), X-ray diffraction (XRD), energy dispersive X-ray spectroscopy (EDX), Raman spectroscopy, and N_2-adsorption measurements. XRD and Raman spectroscopy analyses confirmed the formation of solid solutions with cubic fluorite structure. The catalytic activities of the $Ce_{0.5}M_{0.5}O_2$ (M=Ti, Zr, Hf) nanoparticles were investigated in the low-temperature oxidation of CO. $Ce_{0.5}Zr_{0.5}O_2$ nanospheres exhibit the best performance (100% conversion at 350°C), followed by $Ce_{0.5}Hf_{0.5}O_2$ (55% conversion at 360°C) and $Ce_{0.5}Ti_{0.5}O_2$ (11% conversion at 350°C). Heating the as-prepared $Ce_{0.5}Zr_{0.5}O_2$ to 600°C for extended time leads to a decrease in surface area and, as expected decreased catalytic activity. Depending on the ionic liquid the obtained $Ce_{0.5}Zr_{0.5}O_2$ exhibits different morphologies, varying from nano-spheres in $[C_4mim][Tf_2N]$ and $[P_{66614}][Tf_2N]$ (P_{66614} = trishexyltetradecylphosphonium) to sheet-like assemblies in $[C_3mimOH][Tf_2N]$ (C_3mimOH = 1-(3-hydroxypropyl)-3-methylimidazolium). The microwave synthesis superiority to other heating methods like sonochemical synthesis and conventional heating was proven by comparative experiments where the catalytic activity of $Ce_{0.5}Zr_{0.5}O_2$ obtained by alternate methods such as conventional heating was found to be poorer than that of the microwave-synthesised material.

1. Introduction

Cerium oxide (CeO_2, ceria) and ceria-based materials have attracted significant attention due to their particularly high performance in a variety of applications such as three-way catalysts (TWC) and solid oxide fuel cells (SOFCs).[1] One of the most important properties of ceria is its oxygen storge capacity (OSC): the ability to release and store oxygen under oxidizing and reducing conditions. This metal oxide is able to incorporate more or less oxygen atoms into its crystal lattice depending the temperature and oxygen partial pressure. This is made possible by the low Ce^{3+}/Ce^{4+} redox potential. Advantageous for any application of ceria is its good thermal stability and that it is readily available at low cost.[2]

Ceria on the nanoscale has demonstrated even better performance for oxygen storage owing to the large surface to volume ratio.[3] The oxygen vacancy formation energy is reduced compared to bulk material, which leads to higher surface reactivity at low temperature. An increase in its electronic conductivity is also observed for nanoscale material.[4] The catalytic activity of nano-ceria results from a higher oxygen mobility by creating defect sites.[1] Substitution of Ce^{4+} by Ti^{4+}, Zr^{4+}, Hf^{4+} in CeO_2 leads to solid solutions with a composition of $Ce_{1-x}M_xO_2$ (M= Ti, Zr, Hf) which is found to increase, both, the OSC and ionic conductivity and also has a direct impact on the catalytic activities. The activity is also dependent on other parameters such as the size, morphology and type of dopants.[5]

Microwave heating is a rapid and environmentally friendly option for chemical synthesis. It has been developed as an efficient technology to meet the increasing demand for replacing conventional heat transfer processes. Compared to conventional heating methods, microwave reactions are not only more energy

efficient and faster, but also the reaction product may be obtained even with a higher yield.[6,7] Many different types of materials such as fine chemicals, polymers and inorganic nanomaterials have been effectively synthesised employing microwaves. The two important mechanisms involved during a microwave assisted reaction are dipolar polarisation and ionic conduction.[8] These are the fundamentals, which give rise to a substantial enhancement in heating rate and a reduction in reaction time.

Ionic liquids (ILs), being salts composed of only ions which are liquid at relatively low temperatures (below 100°C) are extraordinarily well suited for microwave reactions. They are receiving increasing attention in recent years for materials synthesis because of their special properties. The possibility to vary the cation and anion as well as the ion combination makes it possible to engineer a solvent with unique properties such as a high ion mobility, low melting points, negligible vapour pressure, good thermal stability, low toxicity, large electrochemical window, non-flammability, and the ability to dissolve a variety of chemicals, in a highly polar yet weakly coordinating solvent.[13,14] In the context of microwave assisted synthesis, ionic liquids feature excellent dielectric properties, which offers great advantages when used as a solvent and reaction medium.[9] There are many types of bulky cations that can be used in ILs which have a high polarisability. The ionic character of the ILs allows them to absorb microwave irradiation even better and energy can be transferred more quickly through this ionic conduction mechanism.

Thus, it is a clear advantage to combine the ILs and microwave heating. The benefits of the duo provide an environmentally friendly, fast, simple and highly efficient route for chemical synthesis[10] which we have now employed for the preparation of $Ce_{0.5}M_{0.5}O_2$ (M= Ti, Zr, Hf) nanoparticles. In this reaction the ionic liquid acts not only as the solvent, reaction medium and, hence, microwave susceptor but also the structure directing agent. We have evaluated the effect of the preparation method, calcination temperature, and the structure of the ionic liquid on the phase purity, crystallinity, morphology and the catalytic activity of $Ce_{0.5}Zr_{0.5}O_2$ where the catalytic activity towards CO oxidation was investigated in detail.

2. Experimental Section

2.1 Materials

All reagents employed were commercially available and directly used without further purification. The ionic liquids 1-butyl-3-methylimidazolium [C_4mim], 1-(3-hydroxypropyl)-3-methylimidazolium [C_3mimOH], tetradecyltrihexyl phosphonium [P66614] bis(trifluoromethanesulfonyl)amide (Tf_2N) were prepared according to modified common procedures reported in the literature. was prepared according to a literature procedure.[11] Lithium bis(trifluoromethansulfonyl)amide (99%), 1-methylimidazole (99%), ethanol (p.a.), 1-chlorobutane (99%) and titanium isopropoxide (97%) was obtained from Sigma-Aldrich, tetradecyltrihexylphosphonium chloride from Cytec, Canada Inc., 1-chloro-3-hydroxypropane (98%) from Acros, sodium hydroxide (98%), acetonitrile (99.5%), ethylacetate (99%) from J.T.Baker, cerium acetate hydrate (99.9%), cerium(IV)oxide (99.99%) and hafnium (IV) chloride (98%) from ABCR, zirconium(IV)oxynitrate hydrate (99.5%).

2.2 Synthesis of $Ce_{0.5}M_{0.5}O_2$ (Ti, Zr, Hf)

Cerium acetate (0.184 g) and an equimolar amount of zirconium(IV)oxynitrate hydrate (0.134 g) or hafnium(IV)chloride (0.134 g) and sodium hydroxide (0.2 g) was added to 2 ml of the ionic liquid, and stirred for 30 min. For the microwave synthesis, the reaction mixture was placed in a 10 ml glass vessel equipped with a Teflon septum and irradiated for 10 min at 80 °C using a single mode microwave operating at 2455 MHz (CEM Discover, Kamp-Lintfort, D). The irradiation power, time and temperature were computer controlled. The product was separated by centrifugation and washed thoroughly with ethanol and deionized water. After that, the product was dried at 85 °C overnight.

For the sonochemical synthesis, the reaction mixture was irradiated in a glass tube sealed with a screw cap in an ultrasound bath (USC200T, VWR International, 45 KHz and 60 W) at room temperature in ambient air for 9 h. The product was washed thoroughly with acetonitrile and deionized water and dried at 85 °C overnight.

Ionothermal synthsis experiments were performed in 50 ml Teflon© cups enclosed in stainless steel autoclaves (Parr Instrument, USA). The reaction mixture was transferred to the Teflon© cup, and sealed in the autoclave, which was placed into a furnace where it was held at 170 °C for 20 h. Then, the autoclave was cooled in air. The resulting powders were separated by centrifugation, washed with ethanol and deionized water several times, and finally dried at 85 °C overnight.

For preparation of $Ce_{0.5}Ti_{0.5}O_2$, cerium acetate (0.184 g), titanium (IV) isopropoxide (0.165 g), sodium hydroxide (0.2 g) were added to the ionic liquid, [C_4mim][Tf_2N] (2 ml), together with deionised water (1 ml) and stirred for 30 min. The mixtures were placed in the microwave using the above described protocol.

2.3 Characterization

Powder diffraction. Powder X-ray diffraction measurements were carried out on a G670 diffractometer with an image plate detector (Huber, Rimsting, D) operating with MoKα radiation (λ = 0.07107 nm).

Transmission Electron Microscopy (TEM). Transmission electron microscopy was carried out on a H-8100 TEM (Hitachi, Tokyo, Japan) equipped with a Penta FET EDX detector (Oxford Instruments, U.K.). An acceleration voltage of 200 kV was applied. To prepare the samples, a suspension of the sample in ethanol was dropped on a copper or gold grid coated with carbon and then dried in air.

Scanning electron microscopy (SEM). Scanning electron microscopy measurements were performed with a high resolution thermally aided field SEM (Zeiss, LEO 1530 Gemini) with a field emmission gun (FEG) and an acceleration voltage of U_{acc} = 0.2-30 KV. For the SEM measurements the TiO_2 nanopowders were put on a carbon-film, dried under vacuum for 20 min and covered with gold to allow for a better electronic conductivity.

IR spectroscopy. Attenuated total reflection (ATR) spectroscopy

was carried out on an Alpha ATR spectrometer equipped with a diamond crystal (Bruker, Karslruhe, D). Solid samples were pressed on the crystal.

Raman spectroscopy. Raman spectra were obtained at 150 mW on a Bruker IFS-FRA-106/s at room temperature.

UV-vis spectroscopy. UV-Vis spectra were measured at room temperature on a Cary 5000 spectrometer (Varian, Palo Alto, US) in reflection mode.

Brunauer-Emmett-Teller (BET) surface area. Nitrogen physisorption experiments were carried out in modified Autosorb 1C setup (Quantachrome). The sample was thermally pretreated at 200 °C for 2 h in He. The physisorption measurement was performed at the boiling point of liquid N_2 (78 K). The surface area was calculated according to the BET (Brunauer-Emmett-Teller) equation. The pore size distribution was obtained through the BJH (Barrett-Joyner-Halenda) method.

CO oxidation was measured with 100 mg of catalyst in tubular fixed bed reactor with 100 ml/min CO/He feed. The temperarure was ramped up to 773 K with 5 K/min heating rate during the measurement. Analysis of CO and CO_2 in the exhaust was performed with a ABB AO2020 NDIR gas analyser.

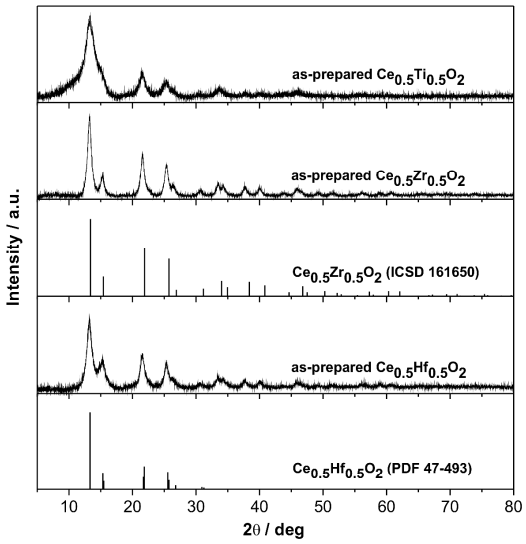

Fig.1 XRD patterns of the as-prepared $Ce_{0.5}M_{0.5}O_2$ (M=Ti, Zr, Hf) samples, database patterns $Ce_{0.5}Zr_{0.5}O_2$ (ICSD 161650) , and $Ce_{0.5}Hf_{0.5}O_2$ (PDF 47-493).

3. Results and Discussion

$[C_4mim][Tf_2N]$ was chosen as it is one of the most common room temperature ionic liquids (ILs) with an appreciably low viscosity. The $[Tf_2N]^-$ anion is known to be weakly coordinating and it should have a comparatively small direct impact on the phase, size and morphology of the reaction products when compared to the cation which is believed to contribute much stronger. [12] $[C_4mim]^+$ represents a short-chain alkyl methylimidazolium cation with an aromatic core which is a highly electron accepting region and is likely to be resposible for the electrostatic attraction with polar moities on the surface of the oxide particles. The acidic protons of the imidazolium head group are likely to be involved in hydrogen bonds.

Conversion of suitable Ce/M precursors in this ionic liquid under microwave irradiation (10 min at 80 °C) led to single phase products with cubic fluorite structure with a composition $Ce_{0.5}M_{0.5}O_2$ (M = Ti, Zr, Hf), see Fig. 1. In the case of $Ce_{0.5}Ti_{0.5}O_2$ the XRD reflections are much broader indicating smaller particle size. Crystalline sizes of synthesized samples were estimated by the Scherrer formula to be 2.9 nm for $Ce_{0.5}Ti_{0.5}O_2$, 5.7 nm for $Ce_{0.5}Zr_{0.5}O_2$ and 4.6 nm for $Ce_{0.5}Hf_{0.5}O_2$. The lattice constants for the three samples deviate significantly from that of pure bulk ceria,[13] from 0.5414 nm to 0.523 (6) nm for $Ce_{0.5}Ti_{0.5}O_2$, 0.528 (3) nm for $Ce_{0.5}Zr_{0.5}O_2$ and 0.527 (6) nm for $Ce_{0.5}Hf_{0.5}O_2$. The decreased lattice dimensions for the three materials agrees well with the change in radius of the tetravalent cations: 0.097 nm for Ce^{4+} compared to 0.064 nm for Ti^{4+} and 0.084 nm and 0.083 nm for Zr^{4+} and Hf^{4+}.[14] The lattice parameter of $Ce_{0.5}Zr_{0.5}O_2$ is very close to that for $Ce_{0.5}Hf_{0.5}O_2$ and agrees well with expected values (Fig. 1). [15,16]

The prepared $Ce_{0.5}M_{0.5}O_2$ (M=Ti, Zr, Hf) was further analyzed by Raman spectroscopy (Fig. 2). The spectrum of CeO_2 is characterized by a sharp Raman mode at 464 cm^{-1} which is due to a symmetrical stretching (F_{2g}) mode of the {Ce-O_8} unit.[17] For the solid solutions $Ce_{0.5}M_{0.5}O_2$ (M=Ti, Zr, Hf) an intense broad band can be found at about 451 cm^{-1} for $Ce_{0.5}Ti_{0.5}O_2$ and 464 cm^{-1} for $Ce_{0.5}M_{0.5}O_2$ (M=Zr, Hf).[18] The F_{2g} mode of $Ce_{0.5}Ti_{0.5}O_2$ is shifted towards a lower frequencies compared to $Ce_{0.5}M_{0.5}O_2$ (M=Zr, Hf) and the reported value for bulk CeO_2,[25] due to the much smaller size of Ti^{4+} compared to Ce^{4+}, Zr^{4+} and Hf^{4+}. Furthermore, for the Ti-containing sample a weak and broad band at 300 cm^{-1} is visible. This may be ascribed to the displacement of oxygen atoms from their ideal fluorite lattice positions.[19]

Analysis of the Raman line width allows to estimate the particle size according to

$$\Gamma(cm^{-1}) = 10 + 124.7/D_R \quad (1)$$

where $\Gamma(cm^{-1})$ is the full width at half maximum of the Raman active mode band and D_R is the particle size. The particle size (DR) of the as-obtained samples ranges from 5.6 nm for $Ce_{0.5}Zr_{0.5}O_2$, to 5.2 nm for $Ce_{0.5}Hf_{0.5}O_2$, to 3.8 nm for $Ce_{0.5}Ti_{0.5}O_2$. The determined values are in good agreement with the crystallite sizes obtained from XRD measurements.

EDX analysis reveals aside from gold and carbon signals that come from the sample preparation only product specific signals which indicates that the samples are pure and free from the ionic liquid.

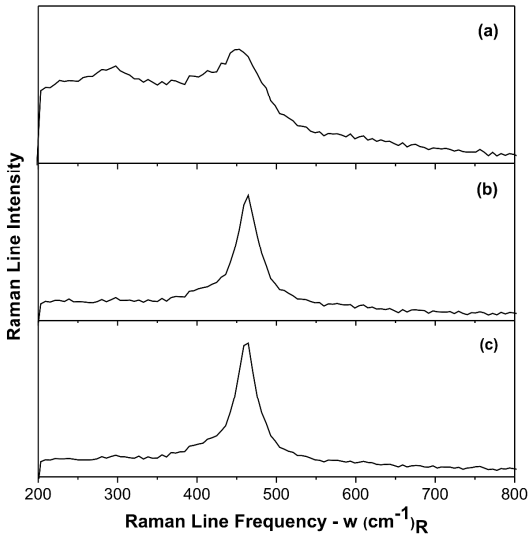

Fig. 2 Raman spectra of the as-prepared $Ce_{0.5}Ti_{0.5}O_2$ (a), $Ce_{0.5}Zr_{0.5}O_2$ (b), $Ce_{0.5}Hf_{0.5}O_2$ (c).

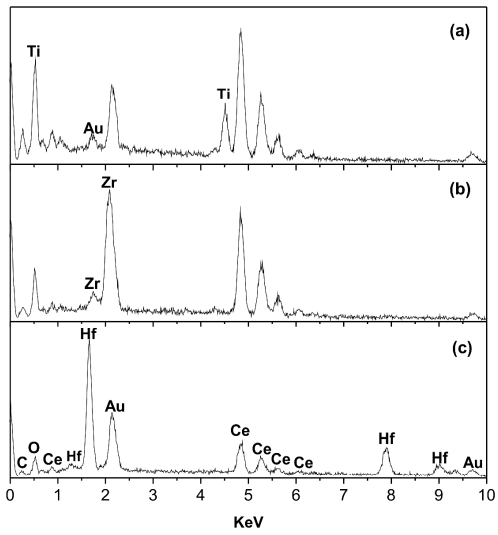

Fig. 3 EDX spectra of the as-prepared $Ce_{0.5}Ti_{0.5}O_2$ (a), $Ce_{0.5}Zr_{0.5}O_2$ (b), $Ce_{0.5}Hf_{0.5}O_2$ (c).

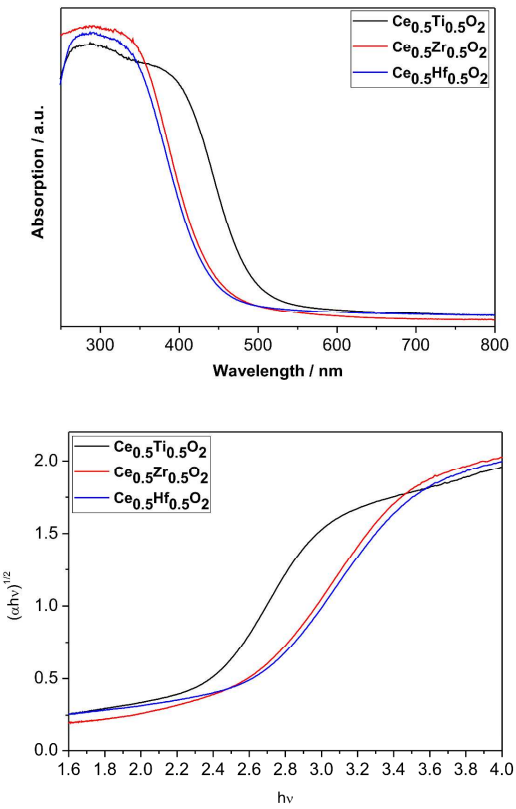

Fig. 4 UV-vis absorption spectra (top) and $(\alpha h\nu)^{1/2}$ –hν (eV) curves for as-prepared samples (bottom).

Table 1. Band gap, particle size as determined from Raman and XRD measurements.

Sample	XRD particle size (nm)	Raman particle size (nm)	Band gap (eV)
$Ce_{0.5}Ti_{0.5}O_2$	2.9	3.8	2.20
$Ce_{0.5}Zr_{0.5}O_2$	5.7	5.6	2.40
$Ce_{0.5}Hf_{0.5}O_2$	4.6	5.2	2.44

The optical absorption spectra of the synthesized samples can be used to determine the optical band gap (Fig. 4 and Table 1). The absorption spectra exhibit an onset at 501.1 nm for $Ce_{0.5}Ti_{0.5}O_2$ for 448.3 nm for $Ce_{0.5}Zr_{0.5}O_2$ and 442.6 nm for $Ce_{0.5}Hf_{0.5}O_2$ (determined by the linear extrapolation of the steep part of the UV absorption towards the base line). The optical band gap (E_g) of the samples can be calculated on the basis of the optical absorption spectra by the following equation

$$(\alpha h\nu)^n = B(h\nu - E_g)$$

where hν is the photo energy, A is the absorbance, B is the related to the effective masses associated with the valence and conduction bands and n is either n=2 for an indirect allowed transition or n=1/2 for the direct forbidden transition. As shown in Fig. 4, bottom. Plotting $(\alpha h\nu)^{1/2}$ versus hν (SI) yields band gaps of about 2.2 for $Ce_{0.5}Ti_{0.5}O_2$ and 2.4 eV for $Ce_{0.5}Zr_{0.5}O_2$ and $Ce_{0.5}Hf_{0.5}O_2$.

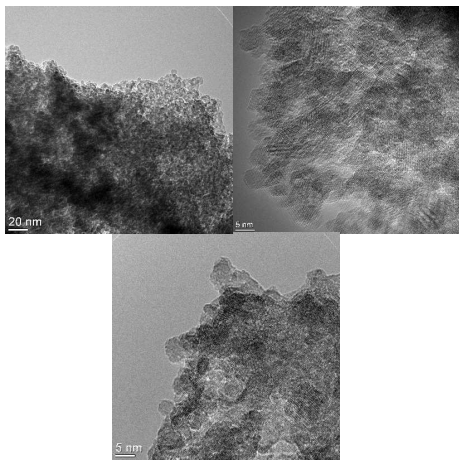

Fig. 5 TEM images of as-prepared $Ce_{0.5}Ti_{0.5}O_2$ (top-left), $Ce_{0.5}Zr_{0.5}O_2$ (top-right), and $Ce_{0.5}Hf_{0.5}O_2$ (bottom).

TEM micrographs show that all samples are composed of aggregated spherical shaped particles with sizes less than 10 nm.

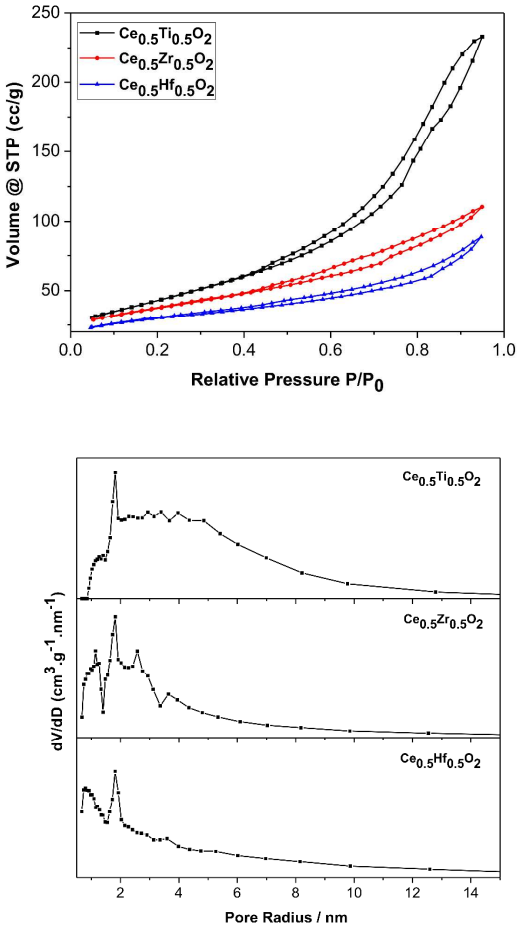

Fig. 6. N_2 adsorption-desorption (top) and pore size distribution curves (bottom) of the as-prepared samples.

The nitrogen adsorption-desorption isotherms and the corresponding pore size distributions of the synthesized samples are shown in Fig. 6; their texture properties are listed in Table 2. The isotherms are of type IV with a hysteresis loop of H1 and H3 type which are characteristic of mesoporous materials. The pore sizes of as-prepared samples are centered at 1.2-4 nm with relatively narrow pore size distribution determined by the BHJ method from the adsorption branch of the isotherms. The pores are formed by the interparticle spaces and not by the porous sturcture of the material as the crystallite size is about 5 nm. The largest pore volume of 0.33 cm^3g^{-1} was observed for $Ce_{0.5}Ti_{0.5}O_2$. Moreover, high surface areas are observed for all samples (Table 2). The specific surface areas range from 162.17 for $Ce_{0.5}Ti_{0.5}O_2$ to 126.23 for $Ce_{0.5}Zr_{0.5}O_2$ and 104.08 m^2g^{-1} for $Ce_{0.5}Hf_{0.5}O_2$. These values are larger than that reported for $Ce_{0.5}Zr_{0.5}O_2$ prepared by high-energy mechanical alloying of pure CeO_2 and ZrO_2 and ceria-doped zirconia prepared by sol-gel synthesis with the use of tetraethylammonium hydroxide.[20,21] However, the surface areas of as-obtained samples are lower than those as-prepared $Ce_{0.5}Zr_{0.5}O_2$ by hydrothermal treatment (190 m^2g^{-1}) and as-prepared $Ce_{0.5}Zr_{0.5}O_2$ by coprecipitation using a cation surfactant hexadecyl trimethyl ammonium bromide.[22,23]

Table 2. Texture properties of the synthesized $Ce_{0.5}M_{0.5}O_2$ (M=Ti, Zr, Hf) samples

Sample	BET surface area, S_{BET} (m^2/g)	Nitrogen pore volume, V_{pore} (cm^3/g)	Pore diameter, from BJH analysis (nm)
$Ce_{0.5}Ti_{0.5}O_2$	162.17	0.33	1.8
$Ce_{0.5}Zr_{0.5}O_2$	126.23	0.165	1.2;1.8; 2.6
$Ce_{0.5}Hf_{0.5}O_2$	104.08	0.129	1.8

The catalytic activities in CO oxidation of the as-prepared $Ce_{0.5}M_{0.5}O_2$ (M=Ti,Zr, Hf) were evaluated and their performance is shown in the Fig. 7. During the course of the CO oxidation, Ce^{4+} is reduced to Ce^{3+}, accompanied by extraction of oxygen from the lattice, which is consumed to oxidise CO to CO_2. The defect mobility of oxygen on the surface has a large influence on the CO oxidation activity and is determined critically by the structure, size and morphology of catalyst. The nanosize of CeO_2 contributes a high surface area to volume ratio, and doping with transition metal oxides could create even more active defect sites and lead to enhanced CO conversion.

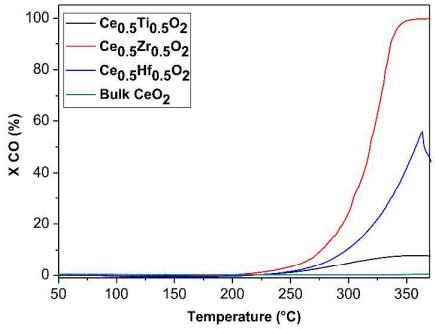

Fig. 7 Catalytic activity for CO oxidation of the as-prepared $Ce_{0.5}M_{0.5}O_2$ (M= Ti, Zr, Hf) in comparison with bulk ceria.

Both the formation of oxygen vacancies and the reduction of Ce^{4+} to Ce^{3+} is thermodynamically more favourable on a ceria surface than in the bulk.[24] Therefore the surface area of the mixed oxide samples provided is very important for CO oxidation. The conversion curves for CO oxidation as a function of temperature are given in Fig. 7 for the as-prepared $Ce_{0.5}M_{0.5}O_2$ (M= Ti, Zr, Hf,) and commercial bulk ceria. The commercial bulk CeO_2 shows little to no activity throughout the whole temperature range tested. It reached only 2% of CO conversion at 450 °C, with an oxidation onset at about 380 °C. Clearly all synthesised mixed oxides achieve much higher catalytic activities and start CO/CO_2 conversion at lower temperatures.

$Ce_{0.5}Ti_{0.5}O_2$ starts converting at 252 °C and reaches a 8% conversion rate at 350°C. For $Ce_{0.5}Zr_{0.5}O_2$ CO conversion starts at 250°C and reaches 100% at 350°C. After reaching the maximum the catalyst activity curves off and stayes at its maximum level indicating a good stability of the catalyst. For the $Ce_{0.5}Hf_{0.5}O_2$, the CO conversion only reaches 55% at about 360 °C at its best. After reaching the maximum the curve drops which shows the catalyst does not possess a good stability at high temperatures.

In view of these results, the order of CO oxidation ability is $Ce_{0.5}Zr_{0.5}O_2 > Ce_{0.5}Hf_{0.5}O_2 > Ce_{0.5}Ti_{0.5}O_2 >$ bulk ceria.

To evaluate the effect of elevated temperatures on phase, particle size and oxidative conversion of carbon monoxide the as-prepared $Ce_{0.5}Zr_{0.5}O_2$ was calcined at 600 °C. From the XRD patterns for the as-prepared $Ce_{0.5}Zr_{0.5}O_2$ and its thermally treated sample (SI. 1), no occurrence of a phase transition can be observed as all of the diffraction peaks match the cubic reference pattern of $Ce_{0.5}Zr_{0.5}O_2$ (ICSD 161650). The particle sizes as estimate using Scherrer's equation increased only slightly from 5.7 nm for the as prepared to 6.0 nm for the calcined sample. However, the specific surface area decreased significantly from 126.23 m^2/g to 40.53 m^2/g after heat treatment at 600 °C (SI. 2) which can be attributed to particle sintering. Fig. 9 shows the CO catalytic activities of the as-prepared and thermally treated $Ce_{0.5}Zr_{0.5}O_2$. It can be seen that the catalytic activity of $Ce_{0.5}Zr_{0.5}O_2$ decreased from 100 % to 80 % after calcination which is an expected trend.[25,26]

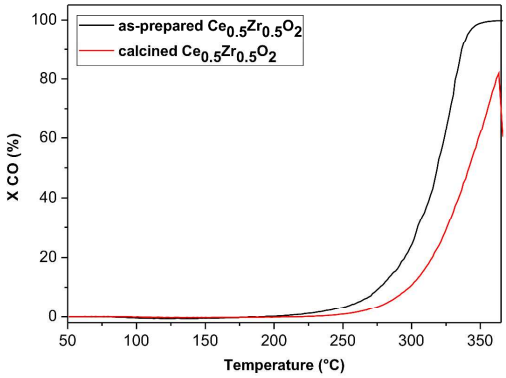

Fig. 8. Catalytic activity for CO oxidation of the as-prepared $Ce_{0.5}Zr_{0.5}O_2$ and its thermally treated sample.

As a superior catalytic activity was found for the $Ce_{0.5}Zr_{0.5}O_2$ material compared to $Ce_{0.5}M_{0.5}O_2$ (M = Ti, Hf), the production of material with the same composition via the other two synthetic approaches (sonochemical (S1) and ionothermal (S2)) in the same ionic liquid were tested.

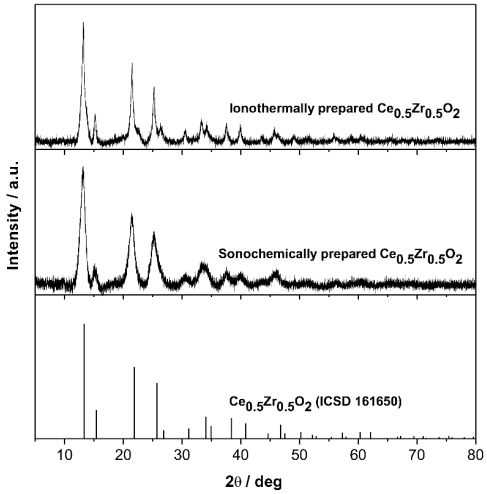

Fig. 9. XRD patterns of as-prepared $Ce_{0.5}Zr_{0.5}O_2$ using different preparation methods in comparison with the database pattern.

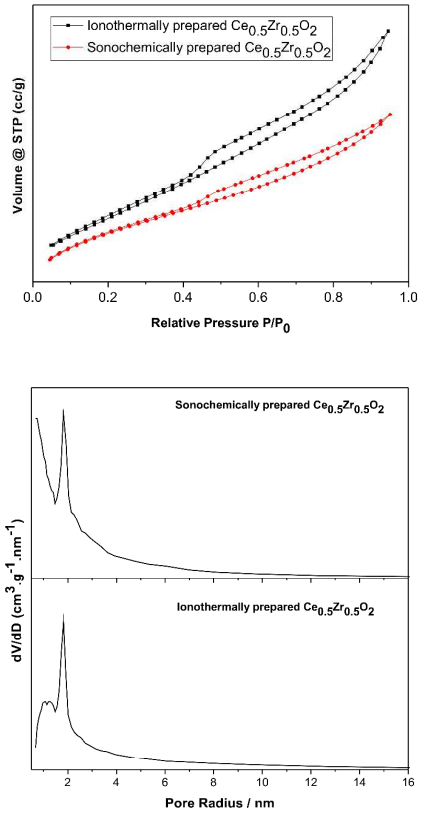

Fig. 10. N_2 adsorption-desorption (top) and (top) pore size distribution curves (bottom) of as-prepared $Ce_{0.5}Zr_{0.5}O_2$ using different preparation methods.

The XRD patterns for the nanoparticles prepared from different synthetic approaches (Fig. 9) share great similarities. All match the database pattern of $Ce_{0.5}Zr_{0.5}O_2$ (ICSD 161650). The particle sizes were estimate using Scherrer's equation and are about 5.6 nm, 3.6 nm and 6.7 nm for the nanoparticles prepared using microwave, ultrasound and ionothermal heating, respectively. The pattern of the sonochemically material clearly shows the broadest diffraction peaks, which implies that the degree of crystallinity of the nanoparticles synthesized using this method is the least probably because of enhanced nucleation rate under the sonochemical-assisted conditions.

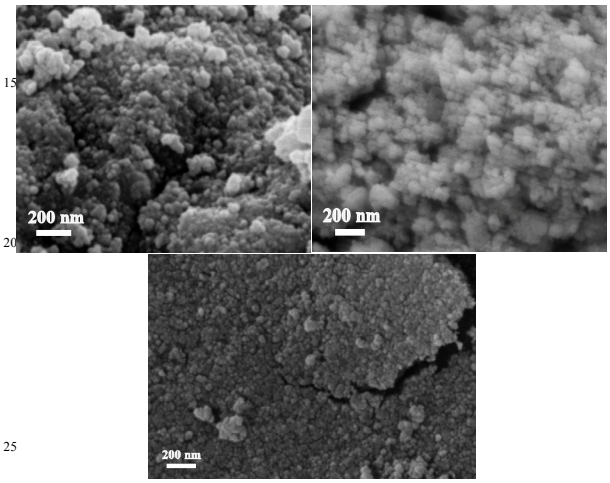

Fig. 11 SEM images of $Ce_{0.5}Zr_{0.5}O_2$ nanoparticles synthesized in $[C_4mim][Tf_2N]$ by (top-left) microwave, (top-right) sonochemical, and (bottom) ionothermal methods.

The SEM images of the $Ce_{0.5}Zr_{0.5}O_2$ prepared from different approaches are shown in Fig.11. From the micrographs the size of the agglomerated $Ce_{0.5}Zr_{0.5}O_2$ NPs prepared sonochemically and ionothermally were estimated to be about 50 nm and 20 nm, respectively. This size is different to what is obtained from the PXRD using Scherrer's equation. This may be due to the fact that the formula estimates the size of single crystalline domains but not the actual size of the agglomerated, polycrystalline nanoparticles.[27] Indeed, observation of the material obtained by microwave irradition by TEM which provides a better resolution confirms small NPs (Fig. 5(top right), whereas SEM micrographs are only able to show the larger aggregates formed (Fig. 11).

The nitrogen adsorption-desorption isotherms and pore size distribution for $Ce_{0.5}Zr_{0.5}O_2$ prepared from different approaches are plotted in Figure 10 and the texture properties are shown in Table 3. The adsorption-desorption isotherms for the samples belong to type IV with hysteresis loops of H3 type. The pore size distribution curve shows that microwave and ultrasound syntheses produce multi-disperse porous nanoparticles. A bi-modal distribution was established for samples prepared via ultrasound (0.7 nm, 1.8 nm) and tri-modal for the microwave prepared samples (1.2 nm, 1.8 nm, 2.6 nm). The nanoparticles prepared ionothermally are rather monodisperse with a pore radius of 1.82 nm. The sonochemically prepared sample shows the largest surface area (139.4 m^2g^{-1}) compared sample prepared via microwave irradiation (126.2 m^2g^{-1}) or using the ionothermal synthesis approach (127.6 m^2g^{-1}).

Table 3. Texture properties of the synthesized $Ce_{0.5}Zr_{0.5}O_2$ samples using different preparation methods.

Sample	BET surface area, S_{BET} (m^2/g)	Nitrogen pore volume, V_{pore} (cm^3/g)	Pore diameter, from BJH Ananlysis (nm)
S1 (ultrasound)	139.4	0.104	0.7;1.8
S2 (ionothermal)	127.6	0.147	1.8
S3 (microwave)	126.23	0.165	1.2;1,8;2.6

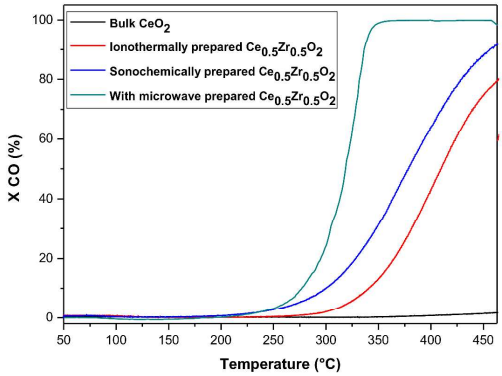

Fig. 12. Catalytic activity for CO oxidation of the as-prepared $Ce_{0.5}Zr_{0.5}O_2$ using different preparation methods in comparison with bulk ceria.

It is found that the material prepared by ultrasound irradiation exhibits a similar CO conversion onset temperature as the microwave-prepared catalyst but it reaches its maximum of conversion (96%) at a much higher temperature (495°C). The ionothermally prepared sample starts the CO conversion at a higher temperature of 300°C and only reaches its maximum of 89% at similar temperature (495°C) to the ultrasound-prepared catalyst. Thus, the materials show a CO oxidation ability in the order: microwave prepared $Ce_{0.5}Zr_{0.5}O_2$ > sonochemically prepared $Ce_{0.5}Zr_{0.5}O_2$ > ionothermally prepared $Ce_{0.5}Zr_{0.5}O_2$ >> bulk ceria.

Reddy et al. investigated the CO oxidation activity of $Ce_{0.5}Zr_{0.5}O_2$ obtained by microwave-assisted synthesis and co-precipitation. It was observed that the microwave synthesized sample showed higher CO oxidation activity (100 %, 525 °C) in comparison to the co-precipitated sample (80 %, 525 °C).[18] Yan et al. determined an activity of 100 % at 500 °C for $Ce_{0.5}Zr_{0.5}O_2$, synthesized via thermolysis at 300 °C using oleic acid and oleylamine as surfactants.[28] Compared to these studies the $Ce_{0.5}Zr_{0.5}O_2$ prepared in ionic liquid via microwave heating reached this conversion at lower temperatures (100 %, 350 °C). Luu et al. [25] determined a CO oxidation activity of 100 % at 350 °C for $Ce_{0.5}Zr_{0.5}O_2$, prepared by the combustion of the gel obtained from mixture of polyvinyl alcohol (PVA) and metal

nitrates at 600 °C. The microwave prepared $Ce_{0.5}Zr_{0.5}O_2$ showed a comparable efficiency but under milder reaction conditions without the need for further treatment such as calcination at high temperature.

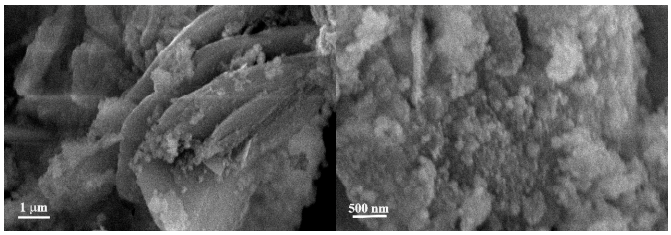

Fig. 13. SEM images of $Ce_{0.5}Zr_{0.5}O_2$ nanoparticles synthesized (left) in $[C_3mimOH][Tf_2N]$, and (right) in $[P_{66614}][Tf_2N]$.

The kind of ionic liquid used in synthesizing $Ce_{0.5}Zr_{0.5}O_2$ is one of the factors that could affect the morphology and crystallization of $Ce_{0.5}Zr_{0.5}O_2$. It has been reported that it is the cation of the ILs which has a greater impact on the nanomaterials.[29] Dupont et.al. conclude that the Ag-NPs and Au-NPs are stabilized by the interaction of the cation $[C_4mim]^+$ with the M-NP surface. In Raman experiments it was observed that in contrast to the anion the absorption bands of the cation are found at lower frequencies than those resulting from neat ILs indicating a substantial interaction. [30] For WO_3 nanoparticles, the presence of the hydrogen bonding between the C2-H of the imidazolium ring and the oxygen of the metal oxide nanoparticles was verified by Raman measurments. [31] For Co–NPs and Mn–NPs prepared in the functionalized IL 1-methyl-3-(3-carboxyethyl)-imidazolium tetrafluoroborate $[EmimCO_2H][BF_4]$, it was found that the stabilization of M-NPs takes place through the cation via its functional group.[32] For Ni-NPs, according to SAXS analysis the increase of the alkyl side-chain of the imidazolium ring from C_4 to C_{14} leads to a decrease in size and in distance between Ni-NPs.[33] To investigate the influence of the cations on the formation of $Ce_{0.5}Zr_{0.5}O_2$, $[C_3mimOH]^+$, and $[P_{66614}]^+$ with the anion bis(trifluoromethylsulfonyl)amide, $[Tf_2N]^-$ were used. $[Tf_2N]^-$ containing ILs are quite chemically stable and low viscous compared to ILs that contain other anions.[34] In addition, this anion is known to be only weakly coordinating, [35] and therefore should have little direct impact on the particle formation and growth. Two cations with substantially different properties , 1-(3-hydroxypropyl)-3-methylimidazolium $[C_3mimOH]^+$ and trishexyltetradecylphosphonium $[P_{66614}]^+$ were chosen for comparative studies: The $[C_3mimOH]^+$ cation contains an imidazolium core like $[C_4mim]^+$ with acidic ring protons, while also bearing a hydroxyl functional group (OH) at the end of the alkyl chain. This is can likely to interact with the surface of nanoparticle through hydrogen bonding. [36] $[P_{66614}]^+$ is a phosphonium based cation with four long alkyl chains attached to it, rendering the cation bulky and hydrophobic. It contains neither acidic proton nor aromatic ring system, and has a highly hydrophobic moiety.

Nano-spherical $Ce_{0.5}Zr_{0.5}O_2$ crystals with an average crystal size of 50 nm are obtained when $[P_{66614}][Tf_2N]$ is used (Fig. 13-right). When $[C_3mimOH][Tf_2N]$ is added to the system, the obtained morphology of $Ce_{0.5}Zr_{0.5}O_2$ is a sheet-like assembly (Fig. 13-left). Fig. (SI-3) presents the XRD patterns of microwave synthesized $Ce_{0.5}Zr_{0.5}O_2$ in different ionic liquids. All diffraction peaks can be indexed to cubic structure of $Ce_{0.5}Zr_{0.5}O_2$ (ICSD 161650). According to Scherrer's formula the sample prepared in $[C_3mimOH][Tf_2N]$ showed the largest crystallite size of 5.5 nm, whereas the sample prepared in $[P_{66614}][Tf_2N]$ showed the smallest size of 4.3 nm. In agreement with previous works concerning the influence of the structure of ionic liquids on formation and stabilization of NPs, the results in this study demonstrate that the structure of the ionic liquid plays a vital impact in determining the crystallinity and the morphology of $Ce_{0.5}Zr_{0.5}O_2$ nanoparticles, and in consequence for their applications in catalyst in order to provide high CO oxidation activity at low temperature.

4. Conclusion

Three types of ceria based catalysts for CO oxidation, $Ce_{0.5}Ti_{0.5}O_2$, $Ce_{0.5}Zr_{0.5}O_2$, $Ce_{0.5}Hf_{0.5}O_2$, were successfully synthesised by microwave reaction in the ionic liquid $[C_4mim][Tf_2N]$. The mixed metal oxides were obtained as highly crystalline materials directly from this synthesis without requiring additional treatment (e.g. calcination). The catalytic activity for CO conversion of all the samples was tested and it was found that $Ce_{0.5}Zr_{0.5}O_2$ shows the best performance. The conversion onset temperature was as low as 250°C and 100% conversion could be achieved at 350°C. At higher temperatures the performance was unchanged, indicative of the high stability of catalyst. $Ce_{0.5}Hf_{0.5}O_2$ and $Ce_{0.5}Ti_{0.5}O_2$ showed an optimum conversion of 55% at 370 °C and 11% at 350°C, respectively. Varying the cation of the ionic liquid resulted in a change in the morphology of $Ce_{0.5}Zr_{0.5}O_2$ from nano-spheres in $[C_4mim][Tf_2N]$ and $[P_{66614}][Tf_2N]$, to larger sheet-like assemblies in $[C_3mimOH][Tf_2N]$. It also could be demonstrated that the heating method has a strong impact on the catalytic activity of the obtained material. The catalytic activity of $Ce_{0.5}Zr_{0.5}O_2$ using ionothermal and ultrasound synthesis, respectively, was found to be poorer than that of the microwave-synthesised material. This can be related to the different heating mechanisms: In the microwave heating process a rapid direct heating of the IL takes place through dielectric heating which results in homogeneous nucleation and a comparatively high degree of crystallinity. During sonication of a liquid ultrasonic waves cause high and low-pressure regions: The low pressure stage is associated with the formation and growth of microscopic bubbles. Collapse of these bubbles leads hot spots of extremely high temperatures and pressure.[37] The fast changing local conditions lead to high nucleation rates, but leave little time for crystallization and particle processes. In the ionothermal process indirect heating occurs through heat transfer from outside to the reaction medium which is associated with a slower heating rate.[38] Thus it is clear that via ultrasound irradiation material with a high surface are, but small particle diameter and pore size is obtained, where as the

ionothermal process yields the largest particles. In summary, the microwave reaction conditions favour the formation of the material with the best catalytic activity.

Notes and references

[a] *Anorganische Chemie III, Ruhr-Universität Bochum, D-44801 Bochum*
[b] *School of Chemistry, Cardiff University, Wales, UK*
[c] *Materials Science and Engineering, Iowa State University and Critical Materials Institute, Ames Laboratory, Ames, IA, 50011, mudring@iastate.edu*

† Electronic Supplementary Information (ESI) available: [details of any supplementary information available should be included here]. See DOI: 10.1039/b000000x/

‡ This work is supported in part by the DFG Cluster of Excellence RESOLV and the Critical Materials Institute, an Energy Innovation Hub funded by the U.S. Department of Energy, Office of Energy Efficiency and Renewable Energy, Advanced Manufacturing Office.

[1] H. T. Chen, J. G. Chang, *J. Chem. Phys*. 2010, **132**, 214702-1-214702-6

[2] E. Garbowski, M. Primet, in *Catalysis by Ceria and Related Materials*, Imperial College press, 2002, pp. 407:

[3] S. Deshpande, S. Patil, S. Kuchibhatla, S. Seal, *Appl. Phys. Lett*, 2005, **87**, 133113.

[4] A. Migani, G. N. Vayssilov, S. T. Bromley, F. Illas and K. M. Neyman, *Chem. Comm*, 2010, **46**, 5936.

[5] D. Valechha, S. Lokhande, M. Klementova, J. Subrt, S. Rayalu and N. Labhsetwar, *J. Mater. Chem*, 2011, **21**, 3718.

[6] V. Polshettiwar and R. S. Varma, *Aqueous Microwave Assisted Chemistry*, RSC, Cambridge, 2010, pp. 1-9.

[7] Y. Wharton, *Symposium Series*, 2011, **157**, 117.

[8] R. R. Martinez-Palou, *J. Mex. Chem. Soc*, 2007, **51**, 252.

[9] P. Lidström, J. Tierney, B. Wathey and J. Westman, *Tetrahedron*, 2001, **57**, 9225.

[10] S. Mallakpour and E. Kowsari, *Iranian Polym. J*, 2006, **15**, 239.

[11] P. Webb, M. Sellin, T. Kunene, S. Williamson, A. Slawin, D. Cole-Hamilton, *J. Am. Chem. Soc*. 2003, **125**, 15577.

[12]T. Alammar, H. Noei, Y. Wang, W. Grünert, A.-V. Mudring, *ACS Sustainable Chemistry and Engineering* 2014, *in press;* T. Alammar, I. Hamm, A.-V. Mudring, M. Wark, , *Appl. Catalysis B* 2014, *in press*; T. Alammar, A. Birkner, O. Shekhah, A.-V. Mudring T. Alammar, A.-V. Mudring, *Mat. Lett*.**,** 2009, **63**, 732-735. . Alammar, A.-V. Mudring, *J. Mat. Sci.* 2009, **44**, 3218-3222., *Mat. Chem. Phys.*, 2010, **120**, 109; T. Alammar, A.-V. Mudring, *Eur. J. Inorg. Chem.* 2009, **19**, 2765.

[13] A.E. Nelson, K.H. Schulz, *J. Appl. Surface Science.,* 2003, **210***,* 206.

[14] R. D. Shannon, *Acta. Crystallogr, Sect. A*, 1976, **32**, 751.

[15] G. Zhou, R. J. Gorte, *J. Phys. Chem. B*, 2008, **112**, 9869.

[16] G. Zhou, P. R. Shah, T. Kim, P. Fomasiero, R. Gorte, *J. Catal. Today*, 2007, **123**, 86.

[17] W. Wang, J. Howe, Y. Li, X. Qiu, D. Joy, M. ,Paranthaman, M. Doktycz, B. Gu, *J. Mater. Chem*., 2010, **20**, 7776.

[18] G. Wang, Q. Mu, T. Chen, Y. Wang, *J. Alloy. Compd*, 2010, **493**, 202.

[19] B. M. Reddy, G. K. Reddy, L. H. Reddy, I. Ganesh, *Open. J. Phys. Chem*, 2009, **3**, 24.

[20] E. A. Trusova, A. A. Khrushcheva, K. V. Vokhmintcev, *J. Euro. Ceram. Soc*, 2012, **32**, 1977.

[21] C. d. Leitenburg, A. Trovarelli, F. Zamar, S. Maschio, G. Dolectti, J. Liorca, *J. Chem. Soc. Chem. Commun*, 1995, **5**, 2181.

[22] C. Cau, Y. Guari, T. Chave, J. Larionova, P. Pochon, S. I. Nikitenko, *J. Phys. Chem. C*, 2013, **117**, 22827.

[23] J. Xiaoyuan, L. Zheng, Z. Yu, D. Guanghui, Z. Xiaoming, *Ind. J. Chem*, 2004, **43A**, 291.

[24] T. X. T. Sayle, S. C. Parker, C. R. A. Catlow, *Surf. Sci*, 1994, **316**, 329.

[25] H. Taguchi, S. I. Matsu-ura, M. Nagao, T. Choso, K. Tabata, *Solid. State. Chem*, 1997, **129**, 60.

[26] N. N. Dao, M. D. Luu, *Adv. Nat. Sci*, 2012, **3**, 015014.

[27] X. Chen, J. L. Hutchison, P. J. Dobson and G. Wakefield, Mater. Sci. Eng. B-Adv., 2010, **166**, 14.

[28] H-P. Zhou, R. Si, W-G. Song, C-H. Yan, *J. Solid State Chem*., 2009, **182**, 2475.

[29] T. Alammar and A. V. Mudring, *ChemSusChem*, 2011, **4**, 1796-1804; T. Alammar, H. Noei, Y. Wang A-V. Mudring, *Nanoscale*, 2013, 5, 8045; T. Alammar, O. Shekhah, J. Wohlgemuth, *J. Mater. Chem*., 2012, **22**, 18252.

[30] J. C. Rubim, F. A. Trindade, M. A. Gelesky, R. F. Aroca, J. Dupont, *J. Phys. Chem. C*., 2008, **112**, 19670; H. S. Schrekker, M. A. Stracke, C. M. L. Schrekker, G. Machado, S. R. Teixeira, J. C. Rubim, J. Dupont, J. Colloid Interface Sci, 2007, 316, 189; P. Serp, K. Philippot, Nanomaterials in catalysis, WILEY-VCH, Weinheim, 2013, pp. 207.

[31] H. C. Chang, J. C. Jiang, W. C. Tsai, G. C. Chen, S. H. Lin, *Chem. Phys. Lett*., 2006, **427**, 310.

[32] D. Marquardt, Z. Xie, A. Taubert, R. Thomann, C. Janiak, *Dalton Trans*., 2011, **40**, 8290.

[33] P. Migowski, G. Machado, S. R. Texeira, M. C. M. Alves, J. Morais, A. Traverse, J. Dupont, *Phys. Chem. Chem. Phys*., 2007, **9**, 4814.

[34] J. Jacquemin, P. Husson, A. A. H. Padua and V. Majer, *Green Chem*, 2006, **8**, 172;

[35] A. Babai, G. Kopiec, A. Lackmann, B. Mallick, S. Pitula, S.-F. Tang, A. Babai, A.-V. Mudring, *J. Mol. Liq.* 2014, **92**, 191; A. Babai, S. Pitula, A.-V. Mudring, *Eur. J. Inorg. Chem.* 2010, *31*, 4933 S. Pitula, A.-V. Mudring, *Chemistry – Eur. J.* 2010, *16*, 3355; S. Pitula, A.-V. Mudring, *Phys. Chem. Chem. Phys.* 2010, *12*, 7056; J. Bartosik, A.-V. Mudring, *Phys. Chem. Chem. Phys.*, 2010, **12**, 4005.

[36] J. Jacquemin, P. Husson, A. A. H. Padua and V. Majer, *Green Chem*, 2006, **8**, 172;

[37] D. Chen, S. K. Sharma, A. Mudhoo, Hand book on applications of ultrasound sonochemistry for sustainability, CRC Press, Inc, 2012.

[38] W. Wang, S. Liang, K. Ding, J. Bi, J. C. Yu, P. K. Wang, L. Wu, *J. Mater. Sci*, 2014, **49**, 1893.

Energy efficient microwave synthesis of mesoporous $Ce_{0.5}M_{0.5}O_2$ (Ti, Zr, Hf) nanoparticles for low temperature CO Oxidation in an ionic liquid- a comperative study

Tarek Alammar,[a] Ying-Kit Chow,[a,b] Anja-Verena Mudring*[a,c]

Graphical abstract